Mon. Not. R. Astron. Soc. **000**, 1–14 (2002) Printed 1 February 2008 (MN LATEX style file v2.2)

XMM-Newton X-ray Observations of the Wolf-Rayet Binary System WR 147

S.L. Skinner[1⋆], S.A. Zhekov[2], M. Güdel[3], and W. Schmutz[4]
[1] *CASA, Univ. of Colorado, Boulder, CO 80309-0389 USA*
[2] *Space Research Institute, Moskovska str. 6, Sofia-1000, Bulgaria*
[3] *Paul Scherrer Institute, Würenlingen and Villigen, CH-5235 Switzerland*
[4] *Physikalisch-Meteorologisches Observatorium Davos, Dorfstrasse 33, CH-7260 Davos Dorf, Switzerland*

Accepted 2007 April 25. Received 2007 March 26; in original form 2007 March 26.

ABSTRACT
We present results of a ≈20 ksec X-ray observation of the Wolf-Rayet (WR) binary system WR 147 obtained with *XMM-Newton*. Previous studies have shown that this system consists of a nitrogen-type WN8 star plus an OB companion whose winds are interacting to produce a colliding wind shock. X-ray spectra from the pn and MOS detectors confirm the high extinction reported from IR studies and reveal hot plasma including the first detection of the Fe Kα line complex at 6.67 keV. Spectral fits with a constant-temperature plane-parallel shock model give a shock temperature $kT_{shock} = 2.7$ keV ($T_{shock} \approx 31$ MK), close to but slightly hotter than the maximum temperature predicted for a colliding wind shock. Optically thin plasma models suggest even higher temperatures, which are not yet ruled out. The X-ray spectra are harder than can be accounted for using 2D numerical colliding wind shock models based on nominal mass-loss parameters. Possible explanations include: (i) underestimates of the terminal wind speeds or wind abundances, (ii) overly simplistic colliding wind models, or (iii) the presence of other X-ray emission mechanisms besides colliding wind shocks. Further improvement of the numerical models to include potentially important physics such as non-equilibrium ionization will be needed to rigorously test the colliding wind interpretation.

Key words: stars: individual (WR 147) – stars: Wolf-Rayet – X-rays:stars.

1 INTRODUCTION

The WR binary system WR 147 (AS 431) has been observed extensively at optical, infrared, and radio wavelengths. The southern component WR 147S is a WN8 star (van der Hucht 2001). Near-infrared images clearly reveal a second source (WR 147N) located ≈0.64″ north of the WN star which was classified as a B0.5V star by Williams et al. (1997, hereafter W97). An earlier O8-O9 V-III spectral type was proposed on the basis of *HST* observations (Niemela et al. 1998). The E(B−V) values of WR 147N and WR 147S are similar (Niemela et al. 1998), suggesting that they are physically associated.

The distance determined from near-IR photometry by Churchwell et al. (1992, hereafter C92) is 630 ±70 pc, which we adopt here for consistency with our previous *ASCA* + *VLA* study (Skinner et al. 1999, hereafter S99). At this distance the projected separation of 0.64″ equates to 403 ± 45 AU. The physical separation depends on the orbital inclination angle which is uncertain. An early study based on analysis of *VLA* radio images gave $i = 45° \pm 15°$ (Contreras & Rodriguez 1999) but more recent work suggests a lower inclination consistent with $i \approx 30°$ (Dougherty et al. 2003; Contreras, Montes, & Wilkin 2004).

Near-simultaneous *VLA* observations at five different frequencies (S99) clearly show that WR 147S has a strong wind. It is a thermal radio source and its flux density S_ν increases at high frequencies according to $S_\nu \propto \nu^{+0.62}$, as expected for free-free wind emission. The radio-derived ionized mass-loss rate of the WN8 star based on its 1.3 cm flux density and assuming a spherical homogeneous wind (Wright & Barlow 1975) is in the range $\dot{M}$(WR) = (1.9 - 4.0) × 10^{-5} $M_\odot$ yr^{-1} (S99). The lower rate is based on solar abundances and the higher value assumes generic WN abundances.

The radio emission at lower frequencies is dominated by a nonthermal component (C92; Contreras & Rodríguez 1996; Moran et al. 1989; S99). The IR and radio images of

⋆ E-mail: skinners@casa.colorado.edu (SLS); szhekov@space.bas.bg (SAZ); guedel@astro.phys.ethz.ch (MG); werner.schmutz@pmodwrc.ch (WS)

W97 suggest that the nonthermal emission peak lies about 0.″07 south of the IR source WR 147N. This offset is very small but does raise the interesting possibility that the nonthermal radio emission originates in a colliding wind shock standing off the surface of the OB star.

X-ray emission from WR 147 was detected by the *Einstein* observatory (Caillault et al. 1985) and moderate resolution CCD spectra were obtained with *ASCA* (S99). A high spatial resolution *Chandra* HRC-I image analyzed by Pittard et al. (2002) did not provide spectral information but did show that the X-ray emission peak lies at or near the northern source WR 147N. It thus appears that the X-rays originate either in the colliding wind shock region near the OB star or in the OB star itself, and both may contribute.

An analysis of the *ASCA* spectra showed that the X-ray emission is dominated by a relatively cool plasma component at $kT_1 \approx 1$ keV, but a hotter component at $kT_2 > 2$ keV could not be ruled out (S99). It was shown that a colliding wind shock could account for the temperature of the cooler plasma in the WR 147 spectrum but the X-ray luminosity predicted by the colliding wind shock model was a few times larger than observed.

We have obtained higher signal-to-noise observations of WR 147 with *XMM-Newton* that provide improved information on emission lines and X-ray temperature structure. The *XMM-Newton* spectra clearly reveal a high-temperature ($kT_2 > 2$ keV) component in addition to the cooler plasma detected by *ASCA*. Here, we revisit the interpretation of the X-ray emission in light of the new data and summarize results from shock models and discrete-temperature optically thin plasma models.

2 OBSERVATIONS

The *XMM-Newton* observation began on 2004 Nov. 4 at 22:54 UT and ended on Nov. 5 at 05:12 UT. Pointing was centered on WR 147 (J203643.65+402107.3). The European Photon Imaging Camera (EPIC) provided CCD imaging spectroscopy from the pn camera (Strüder et al. 2001) and two nearly identical MOS cameras (MOS1 and MOS2; Turner et al. 2001). The medium optical blocking filter was used. The EPIC cameras provide energy coverage over E ≈ 0.2 - 15 keV with energy resolution $E/\Delta E \approx 20$ - 50. The pn and MOS camera pixel sizes are 4.″1 and 1.″1 respectively. The MOS cameras provide the best on-axis angular resolution with FWHM ≈ 4.3″ at 1.5 keV.

Data were reduced using the *XMM-Newton* Science Analysis System (SAS vers. 7.0). The SAS pipeline processing scripts *epchain* and *emchain* were executed in order to incorporate the latest calibration files available as of January 2007. Event files generated by these scripts were time-filtered to remove ≈4 ksec of PN exposure and ≈3 ksec of exposure per MOS in the middle of the observation that were affected by high background radiation. After removing the high-background segments we obtained 16.95 ksec of usable pn exposure and 19.64 ksec of exposure per MOS.

Spectra and light curves were extracted from circular regions of radius $R_e = 25''$ centered on WR 147, corresponding to ≈80% encircled energy at 1.5 keV. Background files were extracted from circular source-free regions near the source. The number of net counts in the background-subtracted spectra were: 4436 (pn), 2085 (MOS1), and 2063 (MOS2). Spectra were binned to a minimum of 20 counts per bin for analysis. The SAS tasks *rmfgen* and *arfgen* were used to generate source-specific response matrix files (RMFs) and auxiliary response files (ARFs) for spectral analysis. The data were analyzed using the *XANADU* software package [1], including *XSPEC* vers. 12.3.0.

3 OBSERVATIONAL RESULTS

We present here the main observational results including images, light curves and spectra.

3.1 X-ray Images

WR 147 was clearly detected by all three EPIC cameras. Figure 1 shows a broad-band (0.5 - 7 keV) EPIC pn image of WR 147 as well as a narrow-band (6.3 - 7 keV) pn image. The latter is dominated by the FeKα emission-line complex at 6.67 keV, which is clearly seen in the spectra (Sec. 3.3).

The centroid position of WR 147 in the broad-band pn image is RA = $20^h\ 36^m\ 43.67^s$, Decl. = +40° 21′ 07.1″ (J2000.0), which is offset by only 0.″3 from its *HST* Guide Star Catalog (v2.2) position (J203643.65+402107.3). We have compared the centroid position of WR 147 in soft (0.5 - 3 keV) and hard (2 - 7 keV) images and find no significant offset. The offset of the X-ray centroid in the FeKα image (Fig. 1) from the Simbad position is only 0.″5, which is less than the raw (unbinned) pixel size.

3.2 X-ray Light Curve

Figure 2 shows the broad-band (0.5 - 7 keV) EPIC pn light curve of WR 147. The mean pn count rate is 0.25 ± 0.03 (1σ) counts s^{-1}. A fit of a constant count rate model to the entire pn light curve (including the 4.1 ksec high-background segment) binned at 400 s intervals gives a probability of constant count rate $P_{const} = 0.45$ (χ^2/dof = 51.5/51). The same fit applied to the last 9.1 ksec of pn data after the high-background subsided gives $P_{const} = 0.54$ (χ^2/dof = 40.4/42). Thus, we find no evidence of significant variability down to 400 s time intervals.

3.3 X-ray Spectra

Figures 3 and 4 show the EPIC pn and MOS1 spectra of WR 147. The spectra are heavily absorbed below 1 keV as previously observed with *ASCA*. This absorption is anticipated on the basis of the known high extinction toward WR 147 (A_V = 11.5 mag, C92; A_V = 11.2 mag, Morris et al. 2000, hereafter M00).

Strong line emission is detected. The most prominent lines along with their laboratory energies and maximum line power temperatures are Si XIII (E_{lab} = 1.865 keV, log T_{max}

[1] The *XANADU* X-ray analysis software package is developed and maintained by NASA's High Energy Astrophysics Science Archive Research Center (HEASARC). See http://heasarc.gsfc.nasa.gov/docs/xanadu/xanadu.html for further information.

= 7.0), S XV (E_{lab} = 2.46 keV, log T_{max} = 7.2), and the FeKα complex which includes Fe XXV (E_{lab} = 6.67 keV, log T_{max} = 7.6). A faint feature that we classify as a possible line detection is Mg XI (E_{lab} = 1.35 keV, log T_{max} = 6.8). Also, there is a hint of Ar XVII (E_{lab} = 3.13 keV, log T_{max} = 7.3) in the MOS spectra, but if present this feature is very weak.

The FeKα line is a new detection and was not seen by *ASCA*. We have generated simulated *ASCA* spectra based on the *XMM-Newton* results which show that the inability to detect the FeKα line with *ASCA* was likely a result of insufficient sensitivity. As Figure 1 shows, the FeKα emission clearly originates in the WR 147 system and is not background related. The presence of the FeKα feature leaves no doubt that very high temperature plasma ($>10^{7.4}$ K) is present in this binary system.

4 STELLAR PROPERTIES

The assumed values of stellar properties relevant to our analysis are summarized below.

4.1 Abundances

We assume solar abundances for the OB star and adopt the values of Anders & Grevesse (1989). Abundances of the WN star are expected to be nonsolar because of its advanced evolutionary state. The X-ray spectra do not constrain the abundances of H, He, C, N, O and their values were held fixed during spectral fits at values appropriate for WR 147 (Table 1 notes). The H and He abundances are from M00 and give the number ratio He:H = 2.5:1. The adopted C, N, and O abundances are generic WN abundances taken from van der Hucht et al. (1986; hereafter vdH86) and reflect the strong overabundance of nitrogen anticipated in WN stars.

The abundances of Ne, Mg, Si, S, Ar, Ca, and Fe do in general affect the X-ray fits and their abundances were allowed to vary in the fitting procedure. The starting values for the abundances of Mg, Si, S, Ar, and Fe were initialized at the canonical WN abundances of vdH86 and those of Ne and Ca were initialized to the values determined for WR 147 by M00. No obvious X-ray emission lines are detected from Ne or Ca and their abundances are not well-constrained by the X-ray data.

4.2 Mass-loss Parameters

To maintain consistency with earlier work, we have adopted the same mass-loss parameters as in S99, which are: $\dot{M}$(WR) = 4×10^{-5} $M_\odot$ yr^{-1}, v_∞(WR) = 950 km s^{-1}, $\dot{M}$(OB) = 6.6×10^{-7} $M_\odot$ yr^{-1}, v_∞(OB) = 1600 km s^{-1}. The value v_∞(WR) = 950 km s^{-1} is identical to a more recent measurement by M00. The above mass-loss parameters, which we herafter refer to as the *nominal* mass-loss parameters, give a ratio of wind ram pressures $P_{WR}/P_{OB} \approx 36$, placing the wind interaction region at a position coincident with that of the nonthermal radio source near WR 147N. The wind momentum ratio for the above mass-loss parameters is $\eta = [\dot{M}(\mathrm{OB})v_\infty(\mathrm{OB})]/[\dot{M}(\mathrm{WR})v_\infty(\mathrm{WR})] = 0.028$, in agreement with that of Niemela et al. (1998).

4.3 Extinction

The IR studies of M00 and C92 give A_V = 11.2 mag toward WR 147. Our X-ray emission models include an absorption component based on Morrison & McCammon (1983) cross-sections. The X-ray models provide a best-fit value for the neutral hydrogen column density N_H, which was allowed to vary during the fits. We obtain an equivalent A_V using the Gorenstein (1975) conversion $N_H = 2.22 \times 10^{21}$ A_V cm^{-2}. The A_V determined from X-ray spectra is in good agreement with IR values.

5 SPECTRAL ANALYIS

We summarize here spectral modeling results that seek to determine whether the observed X-ray emission is consistent with that predicted for a colliding wind shock.

5.1 Plane-Parallel Shock Models

We have fitted the pn and MOS spectra with a constant temperature plane-parallel shock model *vpshock* (Borkowski et al. 2001) in XSPEC using the latest APED ionization fraction data (neivers 2.0). This is a generic shock model in the sense that it does not directly incorporate mass-loss or orbital data for WR 147. However, the model does account for sophisticated physics including non-equilibrium ionization (NEI) effects. The *vpshock* model assumes equal electron and ion temperatures.

As Figure 5 shows, the *vpshock* model does a remarkably good job of reproduding the EPIC spectra. The best-fit parameters are given in Table 1. The inferred N_H gives A_V = 10.0 [9.1 - 11.4; 90% conf.] mag using the Gorenstein (1975) conversion. This value is slightly less than A_V = 11.2 determined from IR studies but is consistent with IR results to within 90% confidence limits.

The shock temperature kT = 2.7 [2.4 - 2.9; 90% conf.] keV inferred from *vpshock* is slightly larger than expected from CW estimates for WR 147. The maximum shock temperature on the line of centers for an adiabatic shock is $kT_{cw} = 1.95\mu v_{1000}^2$ (Luo et al. 1990), where μ is the mean particle weight (ions and electrons) in the shocked plasma and v_{1000} is the shock velocity in units of 1000 km s^{-1}. For the WN abundances adopted here, μ = 1.16. Thus, kT = 2.7 keV implies a pre-shock wind velocity v = 1093 [1030 - 1132] km s^{-1}. This is only 15% higher than the currently accepted value for the WN star (950 km s^{-1}). Given the difficulty in accurately determining terminal wind speeds and element abundances, this agreement is quite good.

The best-fit *vpshock* model slightly underestimates the flux below 1 keV, more noticeably in the pn fit than in MOS (Fig. 5). This suggests that excess soft emission could be present that is not accounted for by the high-temperature shock, perhaps originating in the OB or WN stars. This motivates us to consider a two-temperature model that also includes a cool emission component.

5.2 Discrete Temperature Models

It is possible that the observed X-ray spectrum is the superposition of a cool stellar component and hot colliding wind

shock plasma. A cool X-ray component ($kT_1 < 1$ keV) may originate in the winds of the OB or WN stars themselves via radiative instability shocks (Lucy 1982; Lucy & White 1980). These early studies considered forward shocks in the wind but later work suggests that stronger reverse shocks may also be present (Owocki, Castor, & Rybicki 1988). At the spatial resolution of *XMM-Newton*, any X-ray emission arising from shocks in the winds of the individual stars cannot be separated from colliding wind X-ray emission.

To test the idea that the observed X-ray emission is the superposition of cool stellar radiative wind shock emission plus a hotter colliding wind component, we have fitted the EPIC spectra with a discrete temperature optically thin plasma *vapec* model using two temperature components (2T *vapec*). The results of this model are shown in Figure 6 and summarized in Table 1. There is indeed some improvement in the fit below 1 keV but overall the fit statistic is nearly identical to that of the plane-parallel shock model. Formally, we cannot distinguish between the two based on goodness-of-fit. For comparison, we note that an isothermal optically thin plasma model (1T *vapec*) does not produce an acceptable fit.

The absorption N_H determined from the 2T *vapec* model is identical to that of *vpshock* and implies $A_V = 10.0$ [9.5 - 10.9; 90% conf.] mag. The derived temperature for the cool component $kT_1 = 0.76$ keV is realistic for radiative-driven wind shocks.

The most noticable difference between the *vpshock* model and 2T *vapec* is that the latter gives a considerably higher temperature for the hot component $kT_2 = 3.6$ [3.2 - 4.1; 90% conf.] keV. If due to colliding winds, this would imply a pre-shock wind velocity of at least 1260 km s^{-1}. This velocity is 33% higher than the currently accepted terminal wind speed of the WN star (950 km s^{-1}). As such, the 2T *vapec* model is more difficult to reconcile with the colliding wind picture unless the terminal wind speed of the WN star is considerably higher than currently believed or the mean particle weight in the WR wind is well above the adopted value $\mu = 1.16$.

5.3 Numerical Colliding Wind Models

The models discussed above do not explicitly account for the colliding wind geometry of WR 147. The geometry and temperature structure of a colliding wind shock as well as its intrinsic X-ray luminosity depend on the mass-loss parameters of the WR and OB components as well as the binary separation. Thus, a realistic model must take these into account.

We have produced synthetic X-ray spectra of WR 147 based on 2D numerical hydrodynamic simulations that directly incorporate mass-loss parameters and binary separation. Our approach is similar to that outlined in previous studies (S99, Myasnikov & Zhekov 1993, Zhekov & Skinner 2000). However, some improvements have been made including use of the latest atomic data in the APED [2] data base. The numerical modeling work is ongoing and further refinements are needed but the summary below does provide some insight that may be valuable as a guide for future work.

[2] http://cxc.harvard.edu/atomdb/

This model assumes that *all* of the observed X-ray emission originates in an adiabatic colliding wind shock, which could be an oversimplification if the stars themselves also contribute. The model assumes equal electron-ion temperatures in the shocked WN and OB star winds. This is appropriate for the WN star (eq. [1] of Zhekov & Skinner 2000) but electron-ion temperature differences could be important in the shocked OB star wind. However, our results show that the shocked OB wind contributes only a small fraction to the absorbed X-ray flux, amounting to ≈12% in the 0.5 - 10 keV range and ≈18% in the 4 - 10 keV range. The numerical simulation also assumes ionization equilibrium and in this respect is different than the plane-parallel shock model *vpshock*, which does account for non-equilibrium ionization (NEI). Incorporation of NEI effects into the numerical hydrodynamic model is computationally expensive but may eventually be necessary to rigorously test the colliding wind model. In our initial simulations we have assumed that the physical separation is equal to the projected separation D = 403 AU and have used the mass-loss parameters given in Section 4.2. But, we do consider below how deviations from these values affect the simulated spectra.

There are two differences between the existing colliding wind models and the data that need to be reconciled before the models can be considered satisfactory. First, the models predict an intrinsic X-ray luminosity that is ≈3.5 times larger than inferred from the spectral data. Second, the models do not account for all of the hard-band flux seen in the spectra in the range 4 - 7 keV (Fig. 7). That is, the observed spectrum is harder than our models predict using nominal mass-loss parameters.

The X-ray luminosity mismatch was also apparent in our analysis of the *ASCA* spectra (S99). This difference could easily be accounted for by uncertainties in the distance, mass-loss parameters and orbital separation. The colliding wind X-ray luminosity scales with mass-loss rate $\dot{M}$, wind speed v, and separation D as $L_x \propto \dot{M}^2 v^{-3.2} D^{-1}$ (Luo et al. 1990; Stevens et al. 1992). The mass loss rates could be a factor of ∼2 lower than assumed if the winds are clumped (M00), which would account for the difference. But, a factor of two reduction is not even required since the true binary separation will be larger than the projected separation 403 AU due to inclination effects. Using the inclination estimates cited in Section 1, $i \approx 30°$ gives D = 465 AU and would require that the assumed mass-loss rates be scaled down by a factor of ≈1.7, while $i \approx 45°$ implies D = 570 AU and gives a scale factor of ≈1.6. For the above scale factors, one would obtain $\dot{M}(\mathrm{WR}) = (2.3 - 2.5) \times 10^{-5}$ $M_\odot$ yr^{-1}.

The fact that the observed spectrum is harder in the 4 - 7 keV range than our current models predict may hold important clues to colliding wind physics and stellar properties. We are able to produce a harder synthetic X-ray spectrum by assuming higher terminal wind speeds. If the WR and OB star wind speeds are increased by 30% to v_∞(WR) = 1235 km s^{-1} and v_∞(OB) = 2080 km s^{-1} then the fit in the 4 - 7 keV range is substantially improved, as shown in Figure 7. But the fit is still not statistically acceptable. Other factors such as NEI effects may thus be important and possible electron-ion temperature differences would need to be accounted for at higher wind speeds and shock temperatures. Implementation of NEI effects in the numerical collid-

ing wind models is beyond the scope of this study and will be addressed in future work.

5.4 Summary of Spectral Model Results

The best spectral fit from the models considered above is obtained with a plane-parallel constant-temperature shock model (*vpshock*). The inferred shock temperature kT = 2.7 keV (T ≈ 31 MK) is close to, but slightly greater than, the maximum colliding wind shock temperature predicted for nominal mass-loss parameters and the adopted abundances. A 2T optically thin plasma model (2T *vapec*) gives nearly as good a fit but converges to a hot-component temperature kT = 3.6 keV (T ≈ 42 MK). This higher temperature is more difficult to reconcile with colliding wind models based on current wind speed estimates, but is not ruled out. Preliminary colliding wind models based on numerical hydrodynamic simulations do not give acceptable fits and further refinements are needed to rigorously test the colliding wind predictions.

6 DISCUSSION

We discuss below the implications of the new X-ray results and compare them with previous observations.

6.1 Long-Term X-ray Behavior of WR 147

A comparison between the X-ray properties of WR 147 determined from *ASCA* spectra obtained in 1995 (S99) and those derived from this *XMM-Newton* observation nine years later is informative. Overall, the best-fit *XMM-Newton* models give results that are in very good agreement with lower signal-to-noise *ASCA* data.

The N_H values determined by *ASCA* and *XMM-Newton* are identical. The fluxes determined from *XMM-Newton* depend somewhat on the model used and on which of the three EPIC spectra are fitted. If all three EPIC spectra are fitted simultaneously (Table 1) then the absorbed X-ray flux is 6% less than the *ASCA* value that was determined from a 2T *mekal* model and the EPIC unabsorbed flux is 33% larger than *ASCA*. If only the higher signal-to-noise EPIC pn spectrum is fitted, then the unabsorbed fluxes between *XMM-Newton* and *ASCA* agree to within 1%. Based on these comparisons, we find no compelling evidence that the X-ray flux of WR 147 has changed significantly in the nine years since the *ASCA* observation.

However, sampling of the X-ray emission of WR 147 in the time domain is sparse. Further X-ray monitoring on shorter timescales of ∼months to a year might be worthwhile to determine if short-term X-ray variability is present. Changes in the centimeter radio flux density of WR 147S by ≈25% on a timescale of ≈1 year have been reported by Contreras & Rodríguez (1999) using matched-beam *VLA* observations. If these changes reflect a change in the mass-loss rate of the WN star then the X-ray luminosity might also be affected, since as already noted (Sec. 5.3), the colliding wind X-ray luminosity is dependent on the mass-loss rate. Changes in orbital separation D can also affect L_x, but these changes will be negligible on the timescales considered here because of the wide binary orbit.

6.2 X-ray Temperatures: How Hot is WR 147?

The nominal wind parameters for the WN star (Sec. 4.2) and mean particle weight $\mu = 1.16$ give a predicted maximum temperature for the shocked WN star wind in a colliding wind shock $kT_{cw} = 1.95\mu v_{1000}^2 = 2.04$ keV or $T_{cw} = 24$ MK. Colliding wind theory predicts the hottest plasma will lie on the line-of-centers between the two stars and cooler plasma off the line-of-centers (Luo et al.1990; Stevens et al. 1992).

Several lines of evidence suggest that the plasma is actually hotter than the above calculation predicts. Both the *vpshock* and 2T *vapec* models converge to higher temperatures than above, and the spectrum is harder than numerical colliding wind models can account for using nominal wind parameters. Very hot plasma is clearly present since the Fe Kα line emits maximum power at $T_{max} \sim 40$ MK but the line can form over a range of temperatures.

If the plasma is in fact hotter than predicted by colliding wind models, how can it be explained? One possible explanation is that the adopted wind speeds or abundances are too low. As we have shown, increasing the wind speeds by 30% significantly improves the spectral fit in the 4 - 7 keV range (Fig. 7). Terminal wind speeds are difficult to determine observationally because for WR stars the wind continues to accelerate beyond radii where spectroscopic wind-speed diagnostics are available (Schmutz 1997).

It could also be that the numerical colliding wind models are oversimplified and don't fully account for important physics. The existing colliding wind models do not incorporate NEI effects. However, the plane-parallel shock model *vpshock* does and it provides a better fit to the high-energy part of the spectrum. This could be a clue that NEI effects are important. This can be the case in young shocks that have not had time to reach ionization equilibrium and the plasma is underionized, or in steady-state shocks just downstream from the shock front. NEI can affect the strength of forbidden lines in He-like triplets and grating spectra may be needed to determine if NEI is in fact present.

Lastly, physical mechanisms other than colliding winds may be at work. Nonthermal processes such as inverse Compton scattering could give rise to hard X-ray (or γ-ray) emission, but there is no strong justification for invoking nonthermal emission since the X-ray emission at higher energies can be fitted satisfactorily with a thermal model (Fig. 6). In addition, Reimer, Pohl, & Reimer (2006) have argued that nonthermal emission would likely be masked by stronger thermal emission in WR 147 and difficult to detect.

A more intriguing possibility is that hot thermal plasma at temperatures of ∼30 - 40 MK due to magnetic processes may be present. Such high temperatures are quite typical of magnetic reconnection processes in lower mass stars. Hot plasma that may be of magnetic origin has also been detected in some high mass stars such as the B0.2V star τ Sco (Cohen et al. 2003). And, the detection of nonthermal radio emission from WR 147N is a signature of magnetic phenomena (S99). The possibility that magnetic phenomena are contributing to the high-temperature X-ray emission detected in WR 147 thus remains open, but is still speculative.

6.3 Multi-Temperature Plasma

It is somewhat surprising that the constant temperature *vpshock* model provides such a good fit of the spectrum. In the colliding wind picture, the plasma is not expected to be constant-temperature since hotter plasma lies along the line-of-centers. The presence of emission lines in the spectra that form over a range of temperatures (Sec. 3.3) is a clear indication that the X-ray emitting plasma is not isothermal.

It is also obvious that any soft emission (kT $<$ 1 keV) that may be present from radiative-instability shocks in the winds of the OB or WN stars is not accounted for in the constant-temperature *vpshock* model. This may explain why the *vpshock* model, as well as the colliding wind model, underestimate the flux at lower energies near 1 keV (Figs. 5 and 7). The 2T *vapec* model places most (82%) of the emission measure in cool plasma at $kT_1 = 0.8$ keV (9 MK) and does a somewhat better job accounting for the emission below 1 keV, but some low-level ($\approx 1\sigma$) fit residuals are still present.

6.4 Implications of Clumped Winds

There is now observational evidence suggesting that the winds of massive WR and O stars are clumped rather than homogeneous. This has been discussed in detail for WR 147 by M00. The most important implication of clumped winds for our X-ray analysis is that the mass-loss rates could be a few times lower than the nominal (unclumped) values given in Section 4.2. If the mass-loss rates are lower then the predicted X-ray luminosity from colliding winds is also lower since $L_x \propto \dot{M}^2 v^{-3.2} D^{-1}$. However, the importance of this effect in wide binaries such as WR 147 depends on the ability of clumps to survive at large distances from the WR star and on their survivability within the wind interaction region itself (Pittard et al. 2006). As we have already noted (Sec. 5.3), the difference in L_x between that inferred from the X-ray apectra and colliding wind predictions could be accounted for by a lower mass loss rate. Some X-ray evidence for lower mass-loss rates consistent with clumped winds has also been presented for the WC + O binary γ^2 Velorum (Schild et al. 2004). But, we do emphasize that L_x also scales inversely with the binary separation D, which is not well-known for WR 147 because of uncertainties in the orbital inclination. A more accurate determination of the inclination is needed to determine the factor by which the homogeneous wind mass-loss rates (Sec. 4.2) should be scaled down to obtain agreement between predicted and observed L_x.

Other factors besides clumping also enter into the uncertainty in mass-loss rates. In particular, the uncertain spectral type and luminosity class of the OB companion (Sec. 1) give rise to uncertainties in its mass-loss rate. We have investigated the sensitivity of our numerical colliding wind models to changes in the assumed OB star mass-loss rate by factors of up to ± 2 relative to the nominal values. Such variations have very little effect on the shape of the simulated spectrum or the χ^2 fit statistic since the shocked WR wind dominates the X-ray emission.

The theory of clumped winds predicts that stochastic X-ray bursts should occur if a clump in the WR wind collides with a clump in the O wind (Cherepashchuk 1990). This offers, at least in principle, an indirect means of detecting wind clumps at X-ray wavelengths and quantifying their properties. However, in practical terms the detection of wind clump X-ray bursts would be a major observational challenge. Clump-clump collisions should be rare (Cherepashchuk 1990) and long-term time monitoring would be needed. Also, high signal-to-noise X-ray light curves would be required to discriminate between random noise and clump-induced stochastic variability. If such a search were conducted, WR 147 would not necessarily be an optimal target because of its wide binary separation. At a projected binary separation of 403 AU and an assumed stellar radius $R_{wr} \approx 20\ R_\odot$ (M00) the wind-wind collision zone occurs at more than 4000 stellar radii from the WR star. The clump number density at such large distances would be reduced due to increasing volume and beyond some distance the wind will start to look approximately homogeneous. Furthermore, there are legitimate questions as to whether clumps could even survive as coherent structures so far out in the WR wind. Closely-spaced WR + O or WR + WR binaries would seem to be more promising candidates for a clump-induced X-ray variability search.

7 SUMMARY

We have presented results of a sensitive *XMM-Newton* X-ray observation of WR 147. The main results are the following:

(i) The X-ray spectrum of WR 147 shows strong absorption below $\approx$1 keV and clear evidence for high-temperature plasma, including a first detection of the Fe Kα emission line complex.

(ii) The extinction $A_V = 10.0$ [9.1 - 11.4] mag determined from the X-ray absorption is in good agreement with IR estimates.

(iii) No significant X-ray variability was seen over the $\approx$20 ksec observation. The observed (absorbed) X-ray flux agrees to within a few percent with that measured by *ASCA* nine years earlier.

(iv) A constant-temperature plane-parallel shock model gives a shock temperature $kT_{shock} = 2.7$ keV (31 MK) which is slightly higher than predicted by colliding wind theory. An equally satisfactory two-temperature optically thin plasma model implies even higher temperatures, which are not yet ruled out. Some cooler plasma (kT $<$ 1 keV) may also be present that most likely originates in either the WN or OB stars, but the X-ray spatial resolution is not sufficient to resolve the system into individual binary components.

(v) The X-ray spectrum is harder than predicted by 2D numerical colliding wind shock models using currently accepted wind parameters. This could reflect inaccurate wind speed or abundance estimates, simplifying assumptions in the numerical models, or hard X-ray production via physical processes other than colliding winds. Further refinements in the numerical hydrodynamic models are needed to incorporate potentially important physics such as non-equilibrium ionization effects.

ACKNOWLEDGMENTS

This research was supported by NASA grants NNG05GB48G and NNG05GE69G. Work at PSI (M.G.) was supported by Swiss National Science Foundation grant 20-66875.01. This work is based on observations obtained with *XMM-Newton*, an ESA science mission with instruments and contributions directly funded by ESA states and the USA (NASA).

REFERENCES

Anders, E., Grevesse, N., 1989, Geochim. Cosmochim. Acta, 53, 197
Borkowski, K.J., Lyerly, W.J., & Reynolds, S.P., 2001, ApJ, 548, 820
Caillault, J.-P. et al., 1985, Nature, 313, 376
Cherepashchuk, A.M., 1990, Sov. Astron., 34, 481
Churchwell, E., Bieging, J.H., van der Hucht, K.A., Williams, P.M., Spoelstra, T.A. Th., & Abbott, D.C., 1992, ApJ, 393, 329 (C92)
Cohen, D.H. et al., 2003, ApJ, 586, 495
Contreras, M.E. & Rodríguez, L.F., 1999, ApJ, 515, 762
Contreras, M.E., Montes, G., & Wilkin, F.P., 2004, Rev. Mex. Astron. Astrof., 40, 53
Dougherty, S.M., Pittard, J.M., Kasian, L., Coker, R.F., Williams, P.M., & Lloyd, H.M., 2003, A&A, 409, 217
Gorenstein, P., 1975, ApJ, 198, 95
Lucy, L.B., 1982, ApJ, 255, 286
Lucy, L.B., White, R.L., 1980, ApJ, 241, 300
Luo, D., McCray, R., MacLow, M.-M., 1990, ApJ, 362, 267
Moran, J.P. et al., 1989, Nature, 340, 449
Morris, P.W. et al., 2000, A&A, 353, 624 (M00)
Morrison, R. & McCammon, D., 1983, ApJ, 270, 119
Myasnikov, A.V., Zhekov, S.A., 1993, MNRAS, 260, 221
Niemela, V.S., Shara, M.M., Wallace, D.J., Zurek, D.R., & Moffat, A.F., 1998, AJ, 115, 2047
Owocki, S.P., Castor, J.I., & Rybicki, G.B., 1988, ApJ, 335, 914
Pittard, J.M. et al., 2002, A&A, 388, 335
Pittard, J.M., Dougherty, S.M., Coker, R.F., O'Connor, E.O., & Bolingbroke, N.J., 2006, A&A, 446, 1001
Reimer, A., Pohl, M., & Reimer, O., 2006, ApJ, 644, 1118
Schild, H. et al., 2004, A&A, 422, 177
Schmutz, W., 1997, A&A, 321, 268
Skinner, S.L., Itoh, M., Nagase, F., & Zhekov, S.A., 1999, ApJ, 394, 405 (S99)
Stevens, I.R., Blondin, J.M., Pollock, A.M.T., 1992, ApJ, 386, 265
Strüder, L. et al., 2001, A&A, 365, L18
Turner, M.J.L. et al., 2001, A&A, 365, L27 van der Hucht, K.A., 2001, New Ast. Rev., 45, 135
van der Hucht, K.A., Cassinelli, J.P., & Williams, P.M., 1986, A&A, 168, 111 (vdH86)
Williams, P.M., Dougherty, S.M., Davis, R.J., van der Hucht, K.A., Bode, M.F., & Setia Gunawan, D.Y.A., 1997, MNRAS, 289, 10
Wright, A.E. & Barlow, M.J., 1975, MNRAS, 170, 41
Zhekov, S.A., Skinner, S.L., 2000, ApJ, 538, 808

Table 1. XMM-Newton Spectral Fits for WR 147

Parameter		
Spectrum	pn+mos	pn+mos
Model	vpshock	2T vapec
N_H (10^{22} cm^{-2})	2.2 [2.0-2.5]	2.2 [2.1-2.4]
kT_1 (keV)	2.7 [2.4-2.9]	0.8 [0.7-0.8]
kT_2 (keV)	...	3.6 [3.2-4.1]
τ (10^{11} s cm^{-3})	1.4 [1.1 - 1.8]	...
EM_1 (10^{54} cm^{-3})	1.52	3.35
EM_2 (10^{54} cm^{-3})	...	0.74
Abundances[a]	varied	varied
Ne	4.1 [0.0 - 16.]	$\leqslant$5.4
Mg	1.8 [0.7 - 3.6]	2.1 [0.9 - 3.5]
Si	4.1 [3.2 - 5.1]	5.3 [4.3 - 6.6]
S	5.9 [5.0 - 7.0]	12. [9.5 - 15.]
Ar	7.1 [4.5 - 9.8]	18. [12. - 26.]
Ca	6.4 [1.5 - 11.]	17. [7.5 - 27.]
Fe	5.9 [4.3 - 8.2]	5.3 [4.2 - 6.5]
χ^2/dof	384/330	389/328
χ^2_{red}	1.16	1.19
F_x (10^{-12} ergs cm^{-2} s^{-1})	1.50 (14.4)	1.52 (11.2)
log L_x (ergs s^{-1})	32.83	32.73
log [L_x/L_{wr}]	-6.4	-6.5

Notes: Based on simultaneous fits of the pn and combined MOS1+2 spectra binned to a minimum of 20 counts per bin using XSPEC v. 12.3.0. Tabulated quantities are the neutral hydrogen absorption column density (N_H), plasma energy (kT), upper limit on the shock ionization timescale ($\tau = n_e t$ where n_e is the postshock electron density and t is the time since the plasma was shocked), emission measure (EM), and element abundances. Brackets enclose 90% confidence ranges. The X-ray flux F_x in the 0.5 - 10 keV range is the absorbed value followed in parentheses by the unabsorbed value. The X-ray luminosity L_x is the unabsorbed value in the 0.5 - 10 keV range. A distance of 630 pc is assumed. The ratio L_x/L_{wr} assumes a luminosity for the WR star log [$L_{wr}/L_\odot$] = 5.65 (Morris et al. 2000).

[a]Abundances are relative to the solar values of Anders & Grevesse (1989) as set in XSPEC using the command *abund angr*. A value of unity means solar abundance. The abundances of He, C, N, O were held fixed at WN values (see text): He = 25.6, C = 0.9, N = 140., O = 0.9. The adopted He abundance by number relative to hydrogen is 25.6 × 9.77e-02 = 2.5 (M00) where 9.77e-02 is the solar He abundance by number relative to hydrogen. The Ni abundance was fixed at its solar value in the absence of specific information, but fits are insensitive to Ni. Spectral lines from Ne, Ar, and Ca are weak or absent in the EPIC spectra and their abundances are thus not well-constrained.

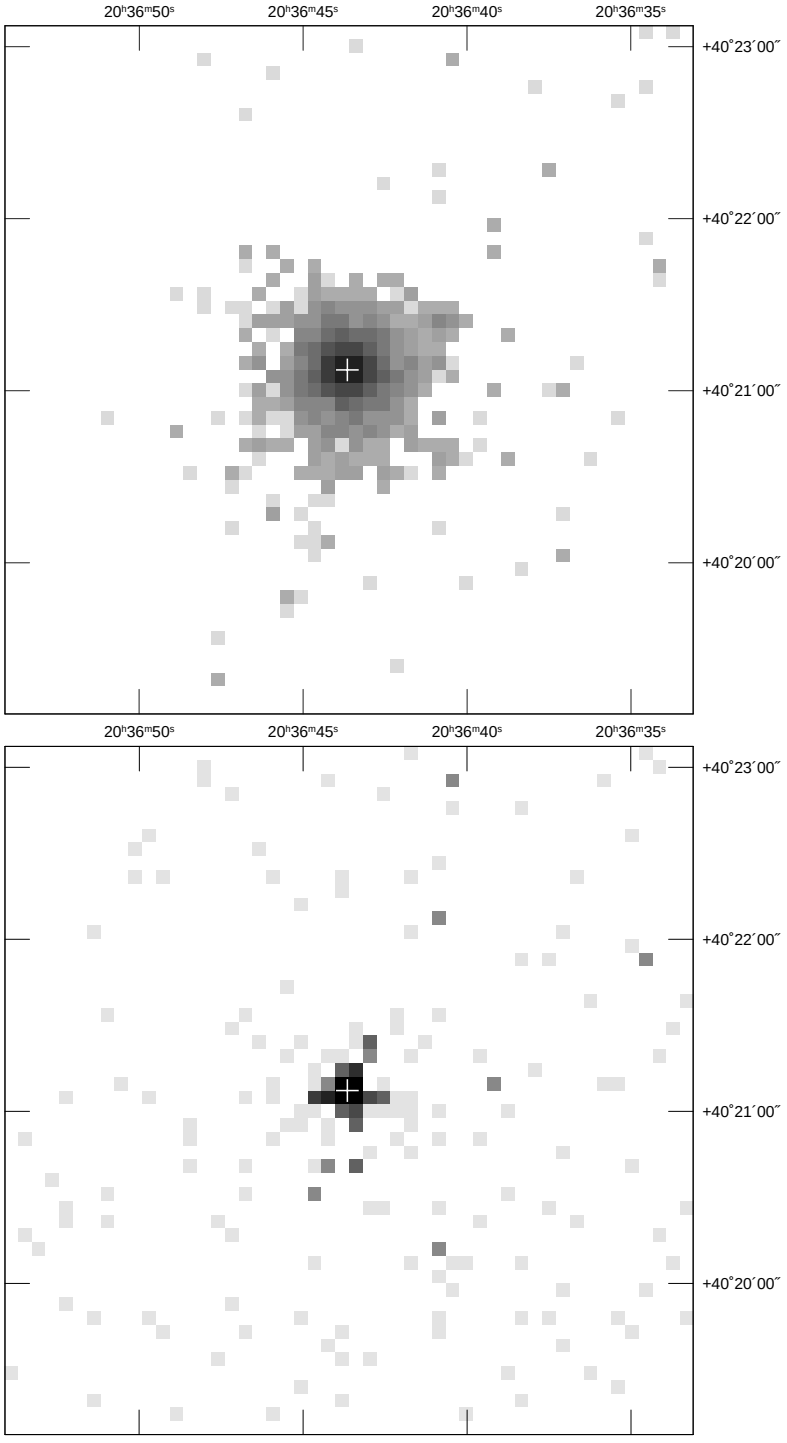

Figure 1. *Top*: EPIC pn image of the region near WR 147 in the 0.5 - 7 keV energy range on a log intensity scale, rebinned to a pixel size of 4.″8 for display. Coordinates are J2000.0 and the cross marks the Simbad position of WR 147. *Bottom*: Same as above only restricted to the 6.3 - 7 keV range, dominated by Fe Kα emission.

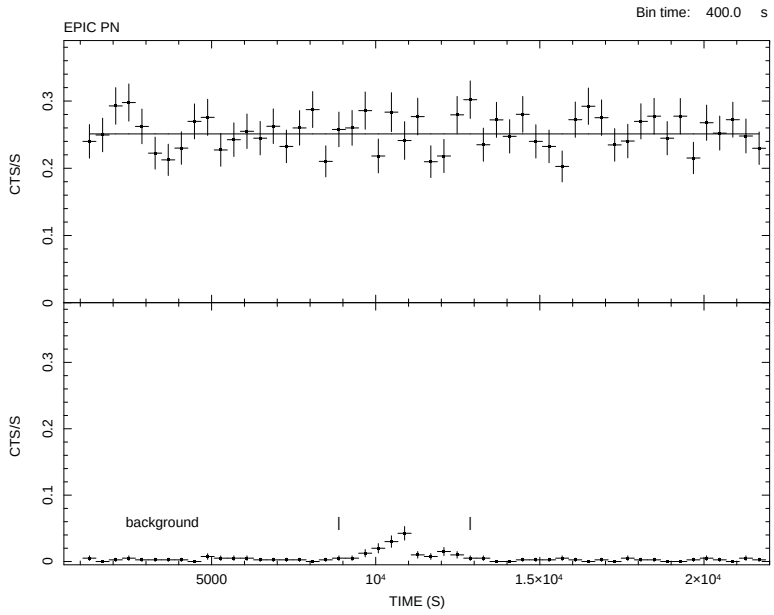

Figure 2. Background-subtracted EPIC pn light curve of WR 147 extracted from a circular region of radius 25″ centered on WR 147 and binned at 400 s intervals. (top panel). The energy range is 0.5 - 7 keV and the solid line is a constant count-rate fit to the data. Error bars are $\pm 1\sigma$. The bottom panel shows the background light curve extracted near the source in the 0.5 - 7 keV range. Vertical bars mark the high-background interval that was excluded from spectral analysis.

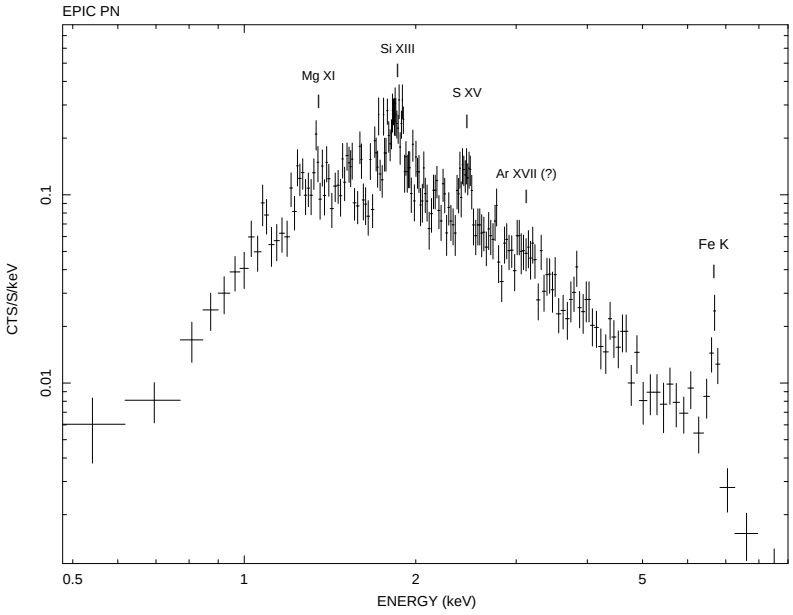

Figure 3. Background-subtracted time-filtered EPIC pn spectrum of WR 147 (4436 net counts) extracted from a circular region of radius 25″ and binned to a minimum of 20 counts per bin.

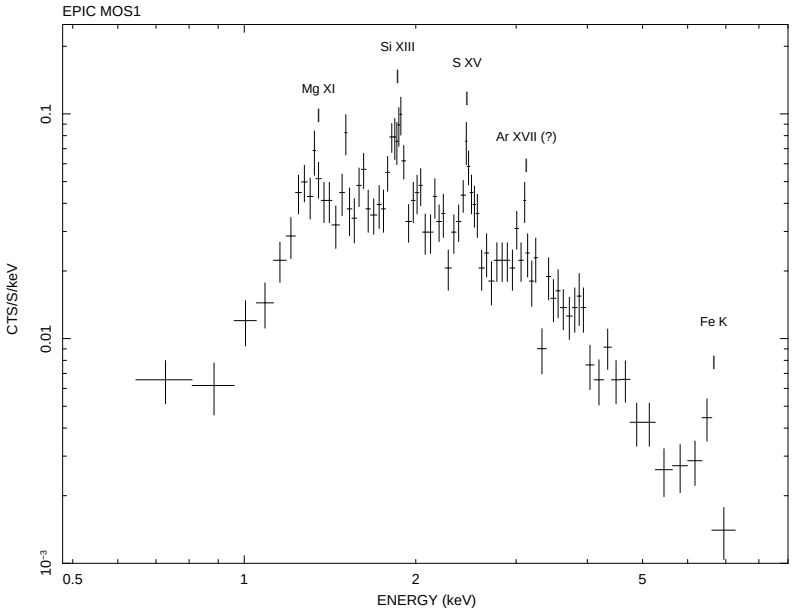

Figure 4. Background-subtracted time-filtered EPIC MOS1 spectrum of WR 147 (2085 net counts) extracted from a circular region of radius 25″ and binned to a minimum of 20 counts per bin.

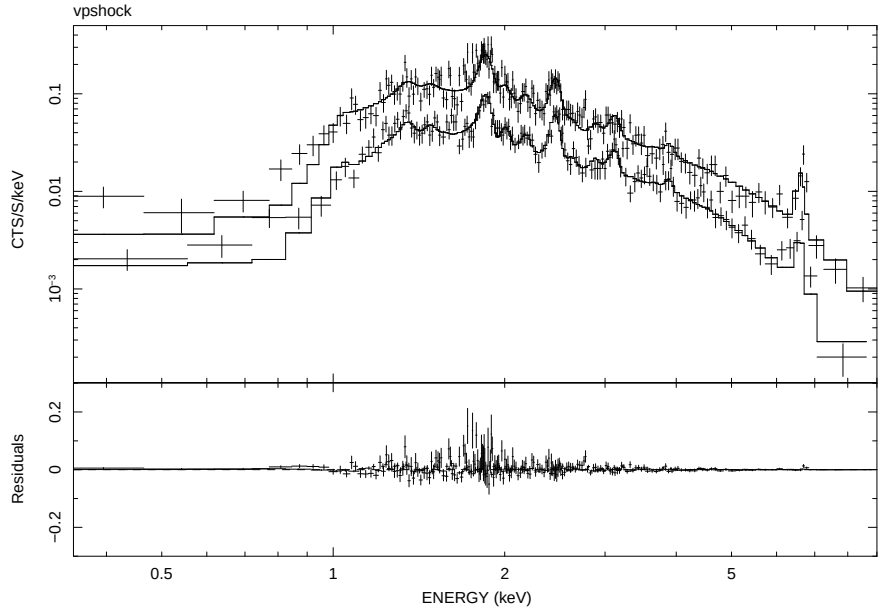

Figure 5. Best-fit plane-parallel shock model *vpshock* (solid line) overlaid on the pn (top) and MOS1+2 spectra (bottom). Fit parameters are given in Table 1. Bottom panel shows fit residuals. Error bars are 1σ.

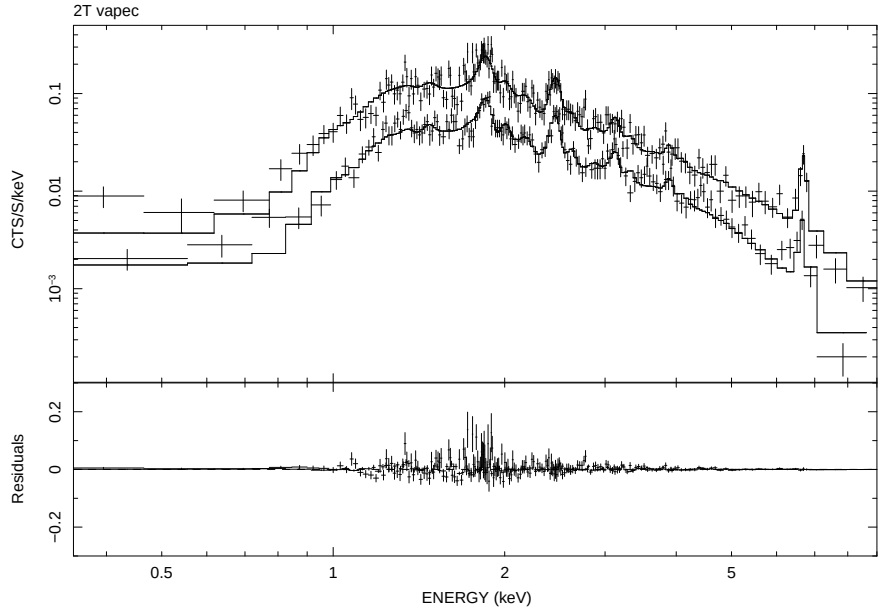

Figure 6. Best-fit two-temperature optically thin plasma model 2T *vapec* (solid line) overlaid on the pn (top) and MOS1+2 spectra (bottom). Fit parameters are given in Table 1. Bottom panel shows fit residuals. Error bars are 1σ.

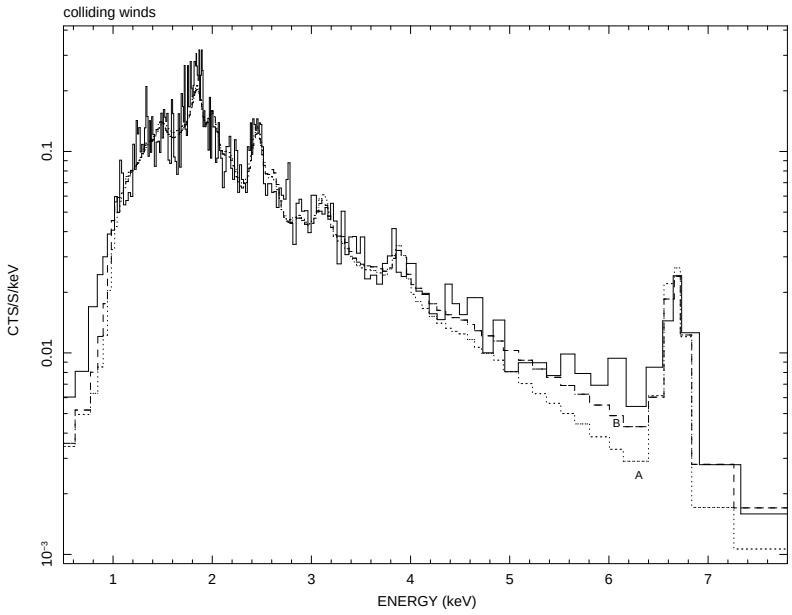

Figure 7. Colliding wind shock models overlaid on the pn spectrum of WR 147 (solid line). The dotted line (A) uses the nominal mass-loss parameters given in Section 4.2 and a wind momentum ratio $\eta = 0.028$. The dashed line (B) assumes 30% higher wind velocities with values v_∞(WR) = 1235 km s^{-1} and v_∞(OB) = 2080 km s^{-1} and leaves the wind momentum ratio unchanged. Error bars have been omitted for clarity and the X-axis scale is linear to accentuate the high energy portion of the spectrum.

This paper has been typeset from a TEX/ LATEX file prepared
by the author.